An Improved DITC Control Method Based on Turn-on Angle Optimization

Chaozhi Huang, *Member, CES*, Wensheng Cao, Zhou Chen, Yuliang Wu, and Yongmin Geng

***Abstract*—Switched reluctance motor (SRM) usually adopts Direct Instantaneous Torque Control (DITC) to suppress torque ripple. However, due to the fixed turn-on angle and the control mode of the two-phase exchange region, the conventional DITC control method has low adaptability in different working conditions, which will lead to large torque ripple. For this problem, an improved DITC control method based on turn-on angle optimization is proposed in this paper. Firstly, the improved BP neural network is used to construct a nonlinear torque model, so that the torque can be accurately fed back in real time. Secondly, the turn-on angle optimization algorithm based on improved GRNN neural network is established, so that the turn-on angle can be adjusted adaptively online. Then, according to the magnitude of inductance change rate, the two-phase exchange region is divided into two regions, and the phase with larger inductance change rate and current is selected to provide torque in the sub- regions. Finally, taking a 3-phase 6/20 SRM as example, simulation and experimental verification are carried out to verify the effectiveness of this method.**

***Index Terms*—Switched Reluctance Motor, Turn-on Angle Optimization, Neural Network, Inductance Change Rate, Torque Ripple.**

I. Introduction

SWITCHED reluctance motor(SRM) has the characteristics of simple structure, low cost[1], [2], which can be widely used in various special occasions. However, the disadvantages of high torque ripple and loud noise limit the application of SRM. There are two main methods to restrain torque ripple at home and abroad, one is to optimize the structure, the other is to optimize the control strategies. In the two methods, optimizing the control strategy is relatively simple and easy to realize.

In literature [3], a control method of three closed-loop structure, which controls by changing the flux linkage, improves the stability of motor operation. In literature [4], the control performance of genetic algorithm and neural network is compared, which proves that artificial neural network has advantages in response time and control performance. In [5], in order to obtain the optimal angle of SRM in dual-mode operation, the relationship between angle and speed is constructed by analytical formula, thus reducing the torque ripple in the optimized area. Literature [6] For the nonlinear parameters of the motor, the artificial neural network is used to establish the parameter model, and the constructed motor identification model is accurate and effective, which can effectively solve the problem of inaccurate parameters. Literature[7]-[10], direct instantaneous torque is used to reduce torque ripple. By detecting the rotor position, the sectors are divided according to the turn-on angle and the turn-off angle, but the influence of the conduction angle on the motor is ignored, which causes the large torque ripple and it is difficult to control under different working conditions. In literature[11]-[14], the torque sharing function (TSF) is used to make each phase torque track the desired torque, so as to reduce the torque ripple. However, this method has certain influence on the current waveform and operation efficiency of the motor, and it is difficult to meet all the performances of the motor at the same time. In [15], in the commutation area, the corresponding compensation changes are made to the functions of the two phases, which makes the TSF more reasonable and reduces the torque ripple. In [16], aiming at the common open circuit fault of SRM, a five-level power converter is designed, which can effectively control the motor when the motor fails. In [17], the optimal commutation control problem is solved by selecting the turn-on angle off-line, but there are some limitations in optimizing the angle off-line. In the literature [18], the conduction angle was optimized for the maximum torque produced per ampere (MTPA). So as to increase efficiency and reduce torque ripple. In [19], the model of flux linkage and torque is constructed by four series, and TSF control method is combined to reduce torque ripple. In [20], the GRNN neural network establishes the mathematical model of flux linkage and realizes the nonlinear and accurate prediction of parameters. In [21], using RBF neural network to construct the nonlinear relationship between different speed, torque, position and current, and it is also used for torque control to reduce torque ripple. By analyzing the characteristics of the small inductance region in the literature [22], the analytical expression of turn-on angle is derived.

On the basis of the conventional DITC control method, this paper presents an improved DITC control method based on turn-on angle optimization. Firstly, the turn-on angle optimization algorithm based on GRNN neural network is

Manuscript received September 25, 2022; revised February 21, 2023; accepted June 02, 2023. Date of publication December 25, 2023. Date of current version July 03, 2023.

This work was supported by National Natural Science Foundation of China under Grant 52167005, Science and Technology Research Project of Jiangxi Provincial Department of Education under Grant GJJ200826. (*Corresponding Author*: *Wensheng Cao*)

Chaozhi Huang, Wensheng Cao, Zhou Chen, Yuliang Wu, and Yongmin Geng are with the School of Electrical and Automation, Jiangxi University of Science and Technology, Ganzhou 341000, China (e-mail: huangchaozhi@163.com, cwscaowensheng@163.com, 1530160926@qq.com, wuyuliang1016@163.com, 569474503@qq.com).

Digital Object Identifier 10.30941/CESTEMS.2023.00043

constructed, so that the turn-on angle of the motor can be adaptively adjusted at different speeds and loads. Then, according to the magnitude of the inductance change rate in the two-phase exchange region, the exchange region is divided into two regions, and in each sub-region, the phase with the larger inductance change rate is preferentially selected to provide torque. Finally, the effectiveness of the proposed method is verified through simulation analysis and prototype experiment.

II. Nonlinear Torque Modeling

The nonlinear torque modeling methods of SRM mainly include look-up table method, analytical method and neural network modeling method. The Look-up table method is to construct a three-dimensional model of $T(i, \theta)$ by using the torque, current and position data obtained by finite element calculation and interpolation. However, the three-dimensional table with large amount of data will cause the speed of table lookup to be slow, and the real-time feedback of torque will be reduced. In the analysis method, the electronic devices are regarded as an ideal device, and the influence of mutual inductance is neglected. However, the analytical method needs to identify more parameters, and the calculation accuracy is not enough. The neural network has good real-time, high accuracy and has certain practicability.

In order to avoid the shortcomings of the above-mentioned look-up table method and analytical method, the improved BP neural network is used to establish the torque model of switched reluctance motor. The nonlinear mapping relationship between current, angle and torque are constructed to realize real-time feedback of torque.

Through finite element simulation of a three-phase 6/20-pole permanent magnet assisted switched reluctance motor, the sample data needed for training the neural network are obtained. The topology of the motor is shown in Fig. 1. In the simulation, the angle range is 0 ~ 18°, and 0.5° is the step length. The current range is 0 ~ 23 A, the step length is 0.1 A, and there are 8547 groups of data.

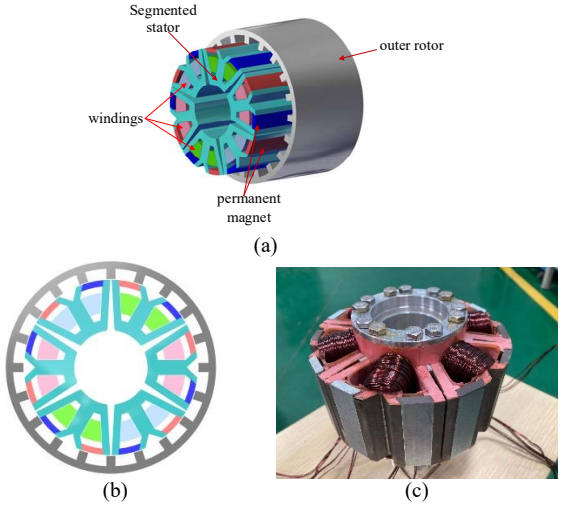

Fig. 1. 6/20 SRM topology. (a) 3D model. (b) Two-dimensional model. (c) Actual prototype.

BP neural network is a feed-forward multilayer unidirectional propagation network, and the layers of forward information transmission and backward error propagation form the learning processes. In practice, it is found that BP neural network has some problems, such as slow convergence rate and unsatisfactory fitting effect. In order to overcome the above shortcomings, this paper combines the adaptive learning method and additional momentum method to form a multi-hidden neural network.

When the additional momentum method is combined in the error handling process, the variation trend of the error will be involved in the calculation, thus avoiding the local extremum.

$$\Delta\omega_{ij}(k+1) = (1-m_c)\eta\delta_i p_j + m_c\Delta\omega_{ij}(k) \tag{1}$$

$$\Delta b_i(k+1) = (1-m_c)\eta\delta_i + m_c\Delta b_i(k) \tag{2}$$

where δ_i represents the residual error, P_j as the output error of j-th output node, Δw_{ij} is the hidden layer weight correction, Δb_i is the threshold correction of each layer, n is the learning rate, m_c is the momentum coefficient.

Where m_c is limited by the sum of squares of errors $E(k)$ in step k, and the specific formula is as follows:

$$m_c = \begin{cases} 0 & E(k) \\ 0.95 & E(k) \\ m_c & \text{other} \end{cases} \tag{3}$$

The adaptive learning method automatically adjusts the learning rate by combining weights and errors in the process of training and learning. So as to improve the prediction accuracy. The concrete formula is:

$$\eta(k+1) = \begin{cases} 1.05\eta(k) & E(k+1)<E(k) \\ 0.7\eta(k) & E(k+1)<E(k) \\ \eta(k) & \text{other} \end{cases} \tag{4}$$

The above improvements and sample data are applied to the training of neural network. With many times of trainings, the neural network structure as shown in Fig. 2(a) is established. The training results and errors are shown in Fig. 2 (c) (d). It can be seen that the error between the training results and the actual torque sample data is small, and the error is basically between -0.5 and 0.5, which realizes the nonlinear mapping of phase current, rotor position angle and motor torque well.

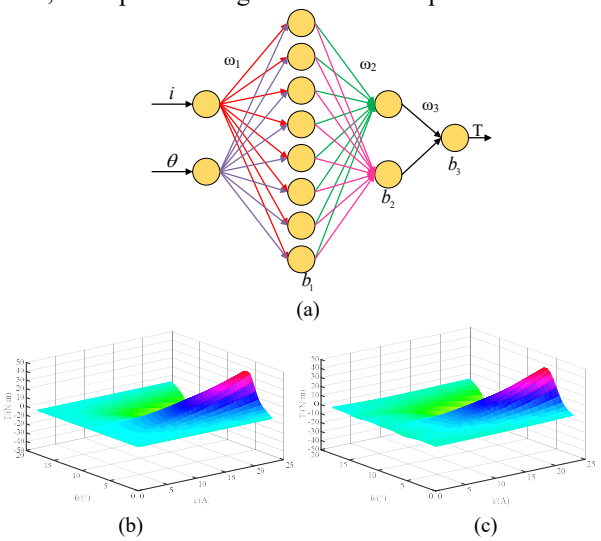

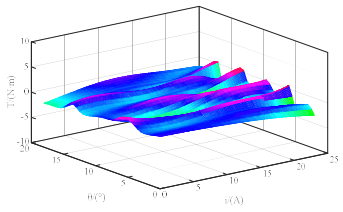

(d)

Fig. 2. Improved BP neural network structure and training result diagram. (a) Improved BP neural network structure. (b) Actual torque surface. (c) Neural network training results. (d) Error surface diagram of training result and actual torque.

III. Conventional DITC Control

Direct Instantaneous Torque Control (DITC) is a commonly used control method to suppress the torque ripple of SRMs. The block diagram of DITC control system is shown in Fig. 3. The DITC control system is composed of torque inner loop and speed outer loop. The system collects the rotor position angle (θ) and current value (i) in real time, and inputs them into the torque estimation unit, and calculates the instantaneous actual torque (T). The torque error (ΔT) obtained by subtracting the actual torque (T) from the reference torque (T_{ref}) gets the switching signals of each phase through the hysteresis controller, so that the torque error (ΔT) is controlled within the corresponding range and the motor run smoothly. The whole system mainly includes power converter, hysteresis controller, torque estimation unit, speed detection and position detection, etc.

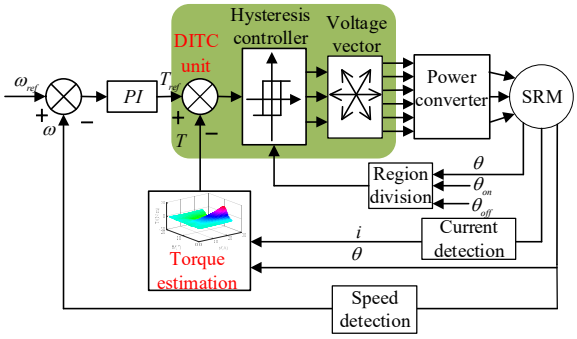

Fig. 3. Conventional DITC control block diagram.

During an electrical cycle of the SRM, each phase turns on and off. The area where torque is supplied by single-phase conduction current is called single-phase conduction region (SPC), and the area where torque is supplied by two-phase conduction current simultaneously is called two-phase exchange region (TPE). In the TPE, the phase in which the current is rising is the excitation phase, and the phase in the falling phase is the demagnetization phase. In the corresponding region, the torque error and the hysteresis controller of each phase output the switching signals of each phase. In TPE, the switch on and off of excitation phase and demagnetization phase are controlled by signals generated by hysteresis of excitation phase and demagnetization phase, respectively. When the torque generated by the excitation phase is too small to bear the total torque, the excitation phase and demagnetization phase need to be conducted together to provide the total torque. In SPC, the switch on and off of the excitation phase is controlled only by the signal generated by the hysteresis of excitation phase.

In the conventional DITC method, the asymmetric half-bridge structure is often chosen as the main body of the power converter, in which each independent bridge arm has two IGBT and two freewheeling diodes. According to the turn-on and turn-off of the two IGBT on each bridge arm, there will be three motor winding states: excitation state 1, zero-voltage freewheeling state 0, and demagnetization state -1, as shown in Fig. 4.

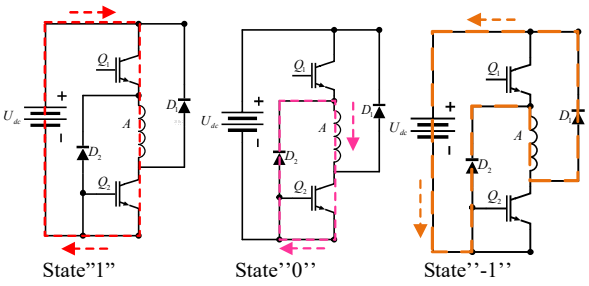

Fig. 4. Three switch states of the power converter.

The conventional DITC method ignores the control of current, resulting in large torque ripple and current spike. In the beginning of TPE, the inductance change rate of excitation phase is small, resulting in small total torque and torque ripple. Then, in order to increase the output of torque, a larger current will be generated. However, at the end of TPE, the change rate of demagnetization phase inductance is large, and the phase current decays slowly, which leads to excessive total torque and torque ripple. In order to reduce torque ripple, an improved DITC control method based on turn-on angle optimization is proposed in this paper, which can effectively suppress torque ripple and improve motor speed and torque performance.

IV. Optimization of Turn-on Angle in TPE

Fig. 5 shows the relationship between different turn-on angles and current, where θ_1 , θ_2 , θ_3 represent the turn-on angles at different positions, θ_{off} is the turn-off angle, and i_1 , i_2 , i_3 are the currents at different turn-on angles . It can be seen from the figure that changing the turn-on angle in DITC system will change the peak value and width of current waveform. The change of turn-on angle will affect the average torque and torque ripple of the motor, and the setting of the turn-on angle is particularly important for torque control and torque ripple reduction.

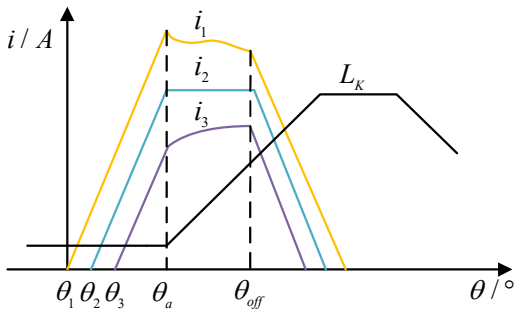

Fig. 5. Relationship between different current, inductance and turn-on angles.

In the conventional DITC control method, the fixed turn-on angle will reduce the adaptability of the motor, and it will produce larger torque ripple when faced with different speeds and load torques. Therefore, this paper presents an algorithm of turn-on angle optimization based on GRNN neural network, which can automatically select the appropriate turn-on angle.

In the actual experiments, BP neural network is suitable for fitting and forecasting large sample data, while GRNN neural network is more advantageous for fitting and forecasting small sample data and unstable data.

The turn-on angle optimization algorithm of GRNN neural network is to generate the turn-on angle based on the speed and load torque. In the data samples required by the neural network, the value range of speed *n* is 300 ~ 1000rpm, with a step of 100, while the value range of load torque *T* is 1 ~ 5N·m, with a step of 1. On the basis of the above speed and load torque, aiming at the minimum torque ripple, through simulation experiments, the optimal turn-on angle under different load torques in a wide speed range is obtained, and finally 40 groups of data are obtained.

A. Improved GRNN Neural Network.

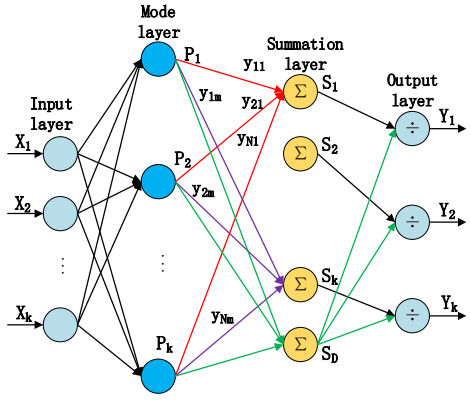

Fig. 6. The structure diagram of GRNN neural network.

Fig. 6 shows the structure diagram of GRNN neural network. It shows that GRNN neural network is mainly composed of four layers: input layer, mode layer, summation layer and output layer. The main workflow of GRNN neural network is as follows.

At first, variables are input from the input layer and then passed to the mode layer. The output of the node of the *i*-th mode layer can be obtained as follows.

$$P_i = \exp\left[-\frac{D_i^2}{2\sigma^2}\right], i = 1,2,\cdots,K \tag{5}$$

$$D_i^2 = (X - X_i)^T (X - X_i), i = 1,2,\cdots,K \tag{6}$$

In the above formula, σ is the smoothing factor, X is the input sample, X_i is the learning sample corresponding to the *i*-th neuron, D_i^2 is the square of the Euclidean distance between X and X_i, and P_i is the output of the *i*-th node.

The summation layer is composed of two units, and the output from the first unit is:

$$S_j = \sum_{i=1}^{N} y_{ij} P_i, j = 1,2,\cdots,K \tag{7}$$

where y_{ij} is the *j*-th element in the output vector Y_i.

The output obtained through the second unit is:

$$S_D = \sum_{i=1}^{N} P_i \tag{8}$$

The final output layer output is:

$$y_j = \frac{S_j}{S_D}, j = 1,2,\cdots,K \tag{9}$$

where y_j is the *j*-th predicted value.

In this paper, the neural network structure of $\theta_{on}(T,n)$ is constructed by the above formula principle. In this structure, the input of the training sample of the neural network is represented by the vector $X_i = [T_i, n_i]^T$ composed of load torque and speed, and the output of neural network is represented by the vector $Y_i = [\theta_i]^T$ composed of the optimum turn-on angle. The input vector $X_i = [T_i, n_i]^T$ passes through the mode layer to get the output P_i of the *i*-th node, then the output S_D and S_j of the summation layer are processed by the summation layer, and the predicted output angle $Y_j = [\theta_j]^T$ is obtained by the output layer. A four-layer neural network structure is constructed, in which the speed and load torque are input and the best turn-on angle is output.

In order to further improve the fitting prediction accuracy of the traditional GRNN neural network, the K-fold cross validation algorithm is added to optimize the GRNN neural network.

The error between the output data of GRNN neural network and the actual data is mainly determined by the smoothing factor σ. Usually, the trial algorithm is used to select the smoothing factor σ, but the trial algorithm is cumbersome and inefficient, resulting in unsatisfactory prediction results. Based on this shortcoming, the K-fold cross-validation is combined with GRNN neural network, so as to improve the fitting generalization ability of the neural network and obtain the best smoothing factor σ.

K-cross validation is to randomly divide data samples into k data groups, and select one of them as the test set, and the other K-1 data groups as the training set. After K cycles, the optimal model is selected by combining the optimal parameters obtained from each data. Here, 8-fold cross-validation is chosen to optimize the model, and the data is scrambled into 8 data groups. One group of data is selected as the test set, and the other 7 groups of data are trained for prediction. Taking the mean square error (MSE) as the standard, by sampling different test sets 8 times at a time without repetition, the σ of the neural network with the best generalization performance of the model was found. The 8-fold-cross verification algorithm is shown in Fig. 7.

B. Construction of Optimization Algorithm for Turn-on Angle

Since the turn-on angle directly affects the performance of torque ripple suppression, the optimal turn-on angle in this paper refers to the turn-on angle corresponding to the small torque ripple at different speeds and different load torques. The acceptable standard of turn-on angle is that the torque ripple is

small under different speeds and loads. The specific optimization process is shown in Fig. 8.

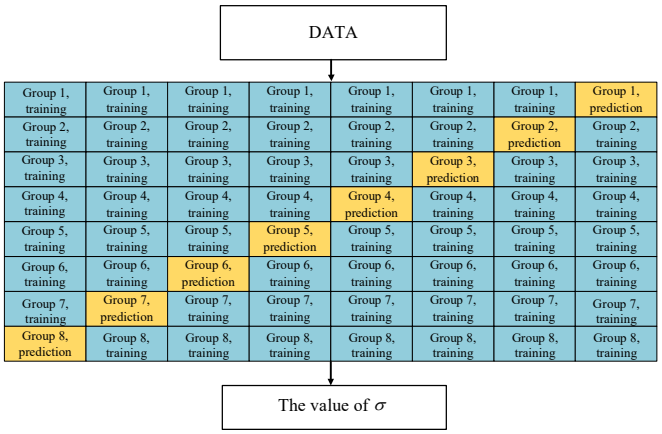

Fig. 7. The 8- fold cross verification algorithm.

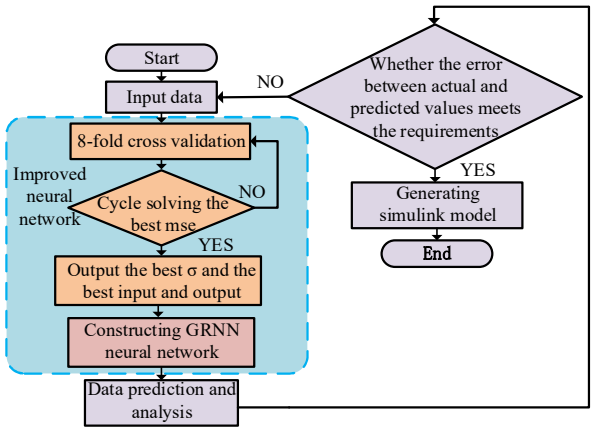

Fig. 8. The training and construction process of GRNN neural network.

The above improvement is applied to the training of turn-on angle optimization, and the fitting results and errors are shown in Fig. 9. As can be seen from Fig. 9(a)-(c), the training results of GRNN neural network is very close to the actual data, and the error is between -0.1 and 0.1, with good fitting effect.

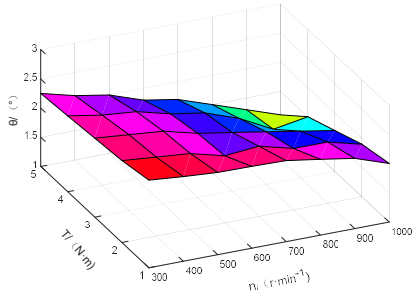

(a)

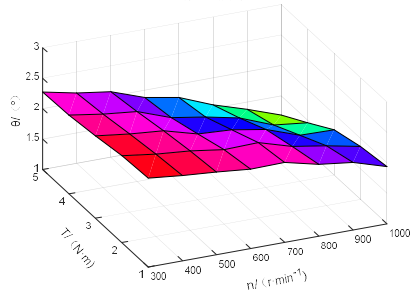

(b)

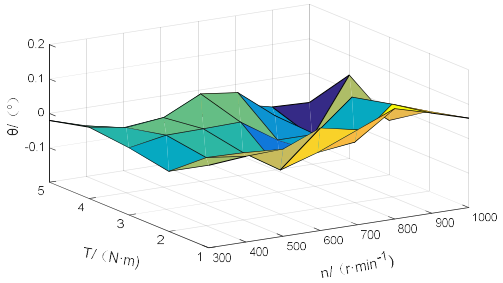

(c)

Fig. 9. The fitting result of GRNN neural network. (a) Actual surface. (b) GRNN neural network fitting result curve. (c) The error between fitting result and actual surface.

According to the results of the optimization algorithm of the turn-on angle, the turn-on angle can be adjusted adaptively according to the speed and load. When the speed or load increases, the turn-on angle will decrease to increase the conducting time, so that the exciting phase current has enough time to rise.

V. Suppression Method of Torque Ripple in TPE

In order to adapt to the optimized turn-on angle, further reduce the torque ripple, this paper presents a new method to suppress the torque ripple in the TPE. Fig. 10 shows the inductance curve from finite element analysis. Take the commutation process of demagnetizing phase A and exciting phase B as an example. It can be seen from the Fig. 10 that, at the beginning of TPE, excitation phase B is in a small inductance region, and inductance change rate $dL/d\theta$ is small. At this time, phase B has just begun to excite, and the current value is small; Mean while, the demagnetizing phase A is in the large inductance region with larger $dL/d\theta$, and the current of phase A at this stage is large. According to torque formula: $T=1/2\times i^2\times dL/d\theta$, phase A has a strong ability to generate torque in the early stage of TPE, so the total torque in the early stage of TPE is mainly provided by phase A.

With the increase of rotor position angle, after the early stage of TPE, the excitation B phase is located in the area with a large $dL/d\theta$, and the current of the phase B are larger at this time, thus increasing the torque supply capacity; At this time, the current of demagnetizing phase A decreases with the shutdown, and the ability of providing torque is weakened. At the later stage of TPE, the total torque is mainly provided by Phase B.

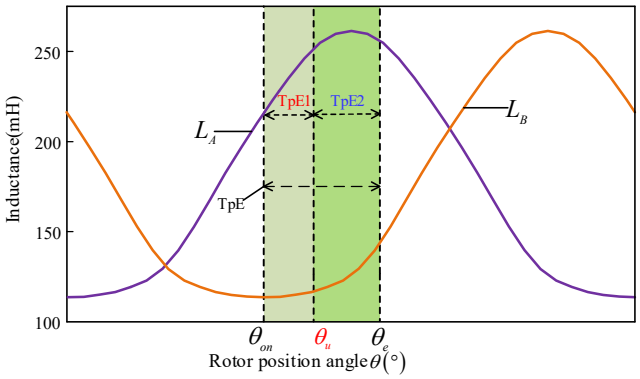

Fig. 10. TPE partition based on inductance characteristics.

In the TPE, the conventional DITC control method is: when the torque is insufficient, the demagnetizing phase will exit the demagnetizing state and enter the freewheeling state, thus controlling the torque of the demagnetizing phase to rise. If the torque still cannot meet the torque required for motor operation, the exciting phase will be excited. When the torque is too large and needs to be reduced, the demagnetizing phase should enter the freewheeling state, and the torque of the demagnetizing phase should be controlled to decrease. If torque still needs to be reduced, the demagnetized phase should be demagnetized.

In the conventional DITC control method, the influence of $dL/d\theta$ on excitation phase and demagnetization phase is not considered in the selection of voltage vector in the TPE, and the demagnetization phase keeps state 1 in the whole TPE, which leads to the total torque not increasing or decreasing in time as required. Therefore, according to the inductance change rate $dL/d\theta$, the TPE can be subdivided into two regions. As shown in the Fig. 10, the demarcation θ_u between the two-phase exchange region 1 (TPE 1) and the two-phase exchange region 2 (TPE 2) is the point where the inductance changes obviously. In the corresponding sub-region, the phase with higher inductance change rate and current is preferred to provide torque, so as to restrain torque ripple. The conduction rules of phase A and phase B in the sub-region are shown in Fig. 11.

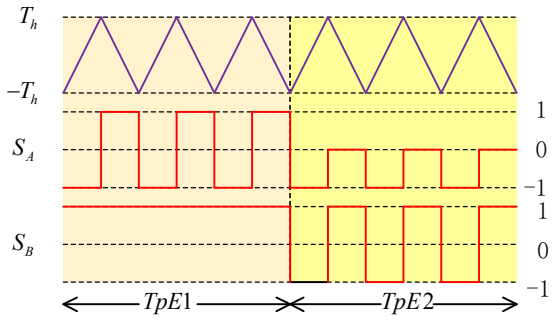

Fig. 11. Voltage vector selection principle.

From the above analysis, it can be seen that the total torque in TPE1 is mainly provided by phase A, and the torque provided by phase B is very small, so phase B keeps conducting in TPE1. When the total torque error T_h exceeds the hysteresis lower limit, the phase A is turned off; When the total torque error T_h exceeds the upper limit of hysteresis, the total torque will be increased by conducting phase A. In TPE2, the total torque is mainly provided by phase B. When the total torque error T_h exceeds the lower limit of hysteresis, both phases are turned off to reduce the total torque. When the total torque error T_h exceeds the upper limit of hysteresis, phase A enters the zero-voltage freewheeling state, and phase B conducts, and the total torque increases. In other TPE, the two-phase conduction rules in TPE1 and TPE2 can be analogized in turn.

As shown in Fig. 12, the control method proposed in this paper constructs a turn-on angle selection algorithm based on neural network, which selects the turn-on angle in real time according to the speed and load torque, and divides the TPE into two regions by the difference of inductance change rate. According to the turn-on angle optimization algorithm and the conduction law of the TPE, the torque control performance in TPE is further optimized.

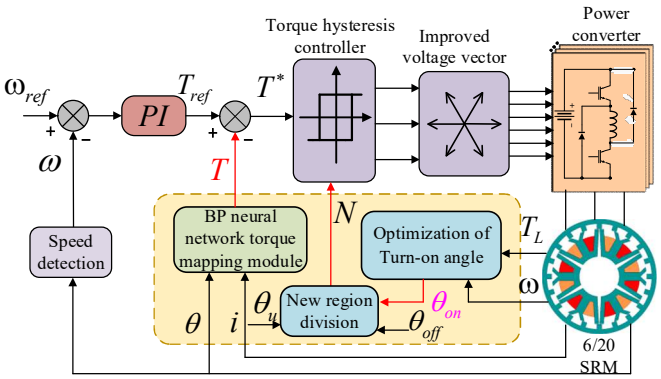

Fig. 12. The control block diagram of the improved DITC control method based on turn-on angle optimization.

VI. Simulation Analysis

A 6/20 SRM model is built in MATLAB/Simulink. The specific parameters of the motor are shown in Table I. In the simulation experiment, the conventional DITC control method and the control method proposed in this paper are compared and analyzed.

TABLE I
MOTOR PARAMETERS

Parameter	Value
Phase number	3
Stator and rotor poles	6/20
Rotor outer diameter (mm)	172
Rotor inner diameter (mm)	143.2
Stator outer diameter (mm)	142
Stator inner diameter (mm)	60
Stack length(mm)	100
Length of air gap (mm)	0.6
Winding turns	55
Minimum inductance (m H)	5.8
Maximum inductance (m H)	13.6
Rated voltage (V)	540
Rated current (A)	30

The torque ripple coefficient is:

$$K_r = \frac{T_{\max} - T_{\min}}{T_{avg}} \tag{10}$$

Where $T_{\max}$ and $T_{\min}$ are the maximum and minimum values of the torque, and T_{avg} is the average value of the torque.

In Fig. 13-Fig. 16, T_e represents the total electromagnetic torque, T_a, T_b and T_c represent the three-phase torque of the motor, i_a, i_b and i_c represent the three-phase current of the motor. In this paper, the total torque is calculated by using the superposition theorem. In TPE, the demagnetization phase current is decreasing, so there is no magnetic circuit saturation phenomenon. Since the phases of switched reluctance motor are independent of each other, there is no cross coupling of flux.

The Fig. 13(a) (b) are the simulation waveforms at a given speed of 400rpm and a load torque of 3N·m. The Fig. 13(a) shows that the torque of the conventional DITC control method is between 3.33-2.42N·m, and the torque ripple is 29%. The conventional DITC method keeps the turn-on angle unchanged. And it is difficult to adapt to the working conditions, resulting

in torque ripple.

However, in the same rotor pole distance, the Fig. 13(b) shows that the torque of improved DITC control method with on-line optimization of turn-on angle is between 3.3 and 2.9 N·m, and the torque ripple is reduced to 13.3%. In the improved DITC control method, when the load torque is 3N·m, GRNN neural network dynamically adjusts the turn-on angle, which can adapt to this situation and reduce the torque ripple. Comparing Fig. 13(a) and Fig. 13(b), it can be seen that the online optimized DITC system can effectively reduce torque ripple.

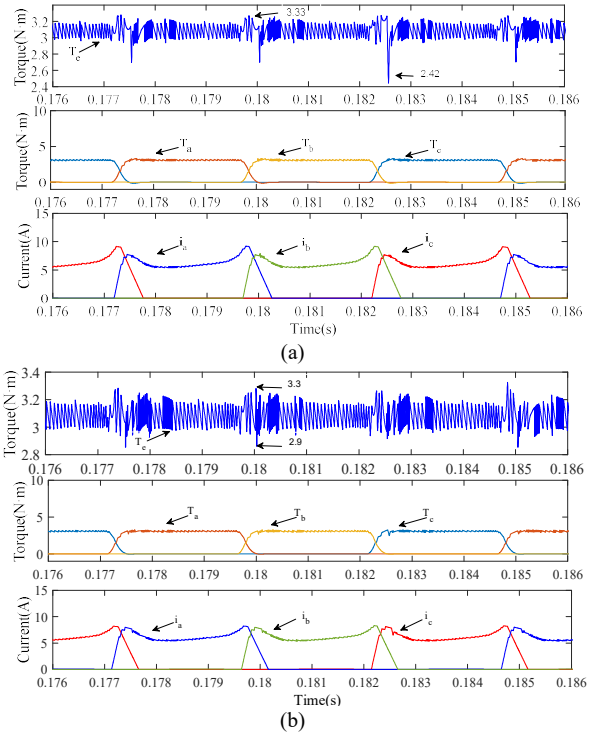

(a) (b)

Fig. 13. Waveform of three-phase current, three-phase torque and total torque (400 r/min, 3 N·m). (a) Conventional DITC method. (b) Improved DITC method.

Then, the influence of different speeds on the torque is compared, as shown in Fig. 14. The results show that: Torque ripple is positively correlated with the increase of speed. Under the condition of fixed load torque, torque ripple intensifies with the increase of speed. As the increase of speed, the torque ripple under the conventional DITC control method increases obviously, while the improved DITC control method based on turn-on angle optimization can still maintain a small torque ripple in the commutation region when the speed increases. When the load torque is fixed, the torque ripple under the improved DITC control method is increased to 21.6% with the increase of the speed, which is 17.7% lower than that under the conventional DITC control method (39.3%). Therefore, the proposed control method can effectively suppress the torque ripple when the speed is increased.

As shown in Fig. 15 the torque ripple of the two control methods is compared when the load torque is 5 N·m and the speed is 400 rpm. When the load torque increases, the proposed control method can still control the torque ripple in a small range (18%), while the torque ripple of the conventional DITC control method is increased to 50%. The proposed control method can effectively reduce the torque ripple when the load torque increases.

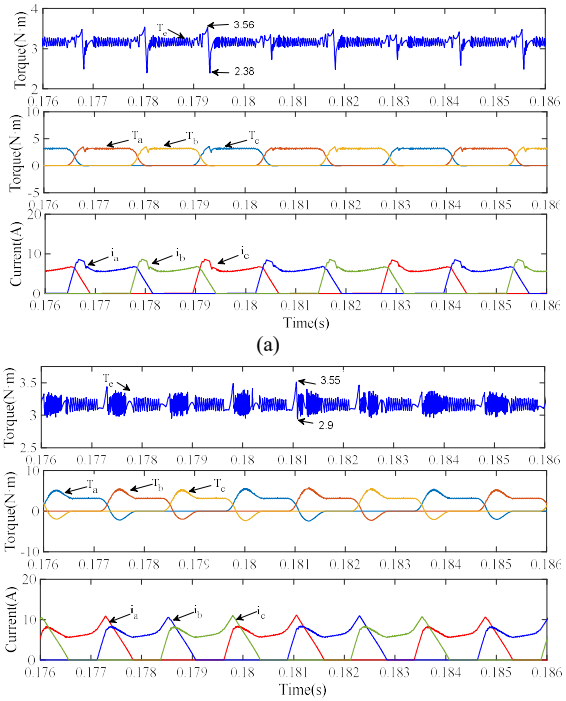

(a) (b)

Fig. 14. Waveform of three-phase current, three-phase torque and total torque (800 r/min, 3 N·m). (a) Conventional DITC method. (b) Improved DITC method.

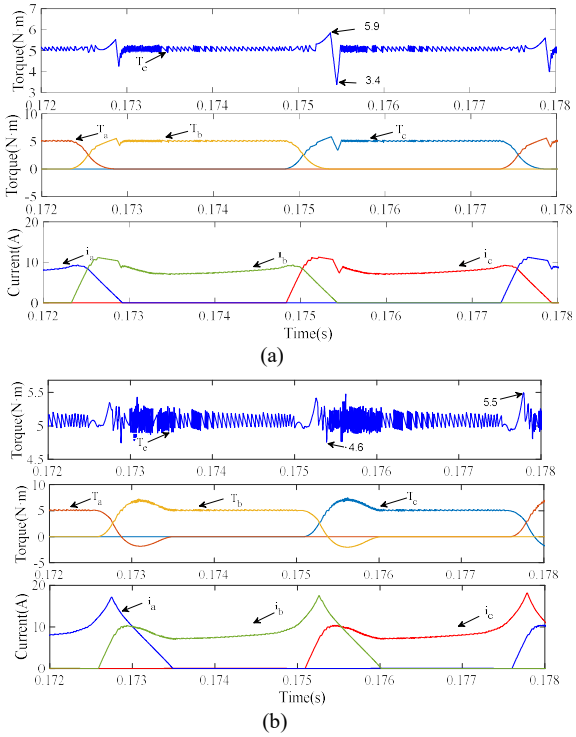

(a) (b)

Fig. 15. Waveform of three-phase current, three-phase torque and total torque (400 r/min, 5 N·m). (a) Conventional DITC method. (b) Improved DITC method.

Fig. 16(a)(b) are the simulation waveform when the load torque is 5N·m, and the speed increases to 800rpm. The Fig. 16(a) shows that the torque of the conventional DITC control method is between 6.3-4.65N·m, and the torque ripple is 33%.

In the conventional DITC control method, the turn-on angle is relatively large, the current rise time is short, and the current value is small. Thus, the torque is low. Because the torque is small, the torque will become larger under the action of the negative feedback of the outer loop. Resulting in a larger total torque and a larger torque ripple.

However, in the same rotor pole distance, the turn-on angle optimization algorithm uses GRNN neural network. When the speed increases, the turn-on angle will be adjusted to a smaller value, which will make the current rise faster. The larger current value will lead to the larger torque, and will not produce a smaller torque. By optimizing the turn-on angle, the total torque is controlled between 5.42-4.9 N·m, and the torque ripple is reduced to 10.4%. The improved DITC system has small torque ripple, which is conducive to the smooth operation of the motor.

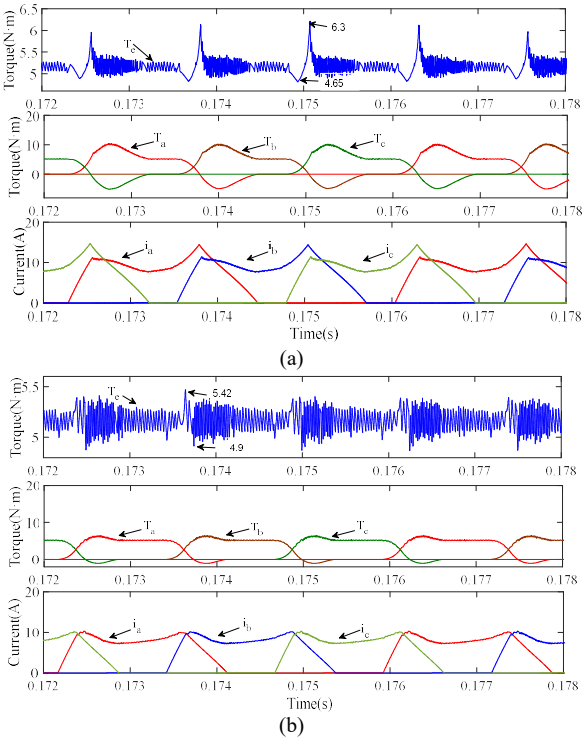

Fig. 16. Waveform of three-phase current, three-phase torque and total torque (800r/min, 5 N·m). (a)Conventional DITC method. (b) Improved DITC method.

The simulation results show that compared with the conventional DITC method, the improved DITC method can effectively reduce the torque ripple under different load torques and speeds. When the load decreases, the turn-on angle can be increased, and when the speed increases, the turn-on angle can be reduced, thus reducing torque ripple.

In order to further verify the influence of the improved DITC control method based on turn-on angle optimization on the torque ripple of SRM, the exponential TSF and CCC control methods are compared with the control method proposed in this paper. The specific performance are shown in Table II.

First of all, when the speed is 400 rpm and the load torque is 3 N·m, the results show that: Compared with the conventional CCC control method and the conventional TSF control method, the control method proposed in this paper is reduced by 19% and 16% respectively. Secondly, when the speed is 800 rpm and the load torque is 5N·m, the control method proposed in this paper is reduced by 35.7% and 30.7% respectively compared with the conventional CCC control method and the conventional TSF control method. It shows that the improved DITC control method proposed in this paper can stably suppress the torque ripple in commutation region when the speed and load torque increase. Therefore, compared with the TSF control method and CCC control method, the improved DITC control method proposed in this paper has a better suppression effect on the torque ripple of SRM at different speeds and loads.

TABLE II
PERFORMANCE COMPARISON OF DIFFERENT CONTROL METHODS

Method	Speed (rpm)	Load torque (N· m)	Torque ripple (%)
Proposed method	400	3	13
TSF	400	3	29
CCC	400	3	32
Proposed method	800	5	17.3
TSF	800	5	48
CCC	800	5	53

VII. EXPERIMENTAL VERIFICATION

The experimental platform of the control system is shown in Fig. 17. The experiment platform mainly includes SRM, magnetic powder brake, control circuit and detection circuit. The controller uses TMS320F28335 DSP of TI Company as the control core, and uses absolute value encoder to measure the rotor position information, and carries out data communication through ECAN bus. The torque is measured by a torque sensor.

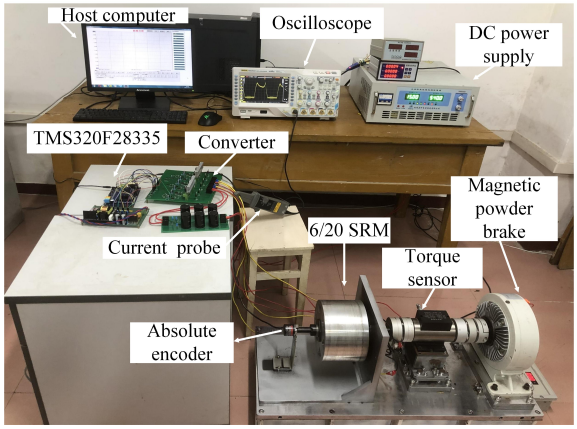

Fig. 17. Structure diagram and assembly drawing of SRM.

The speed is set at 400rpm and the load torque is 3N·m. According to conventional and improved DITC control methods, the experiment was carried out. It can be seen from Fig. 18-19 that the peak current of conventional DITC is about 11A, the torque is in the range of 3.46-2.4 N·m, and the torque ripple is 35.3%. From Fig. 20-21, the peak current of the improved DITC is about 8A, the torque range is 3.4-2.8 N·m, and the torque ripple is 20%. As can be seen from Fig. 18-21, the torque ripple of the conventional DITC control method is obviously larger than that of the improved DTC control method.

Set the speed to 800 rpm and the load torque to 5 N·m, and

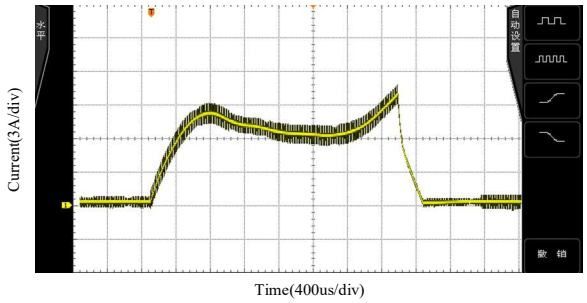

Fig. 18. The current waveform diagram of conventional DITC method.

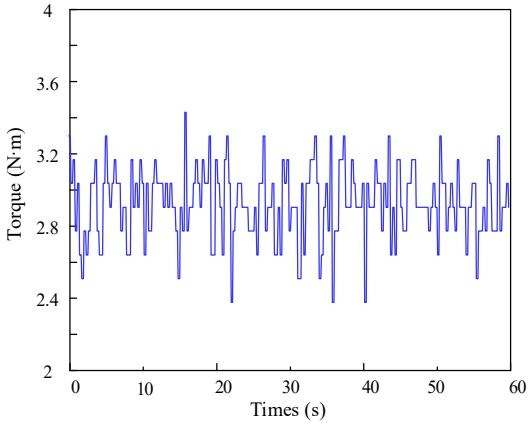

Fig. 19. The torque waveform diagram of conventional DITC method.

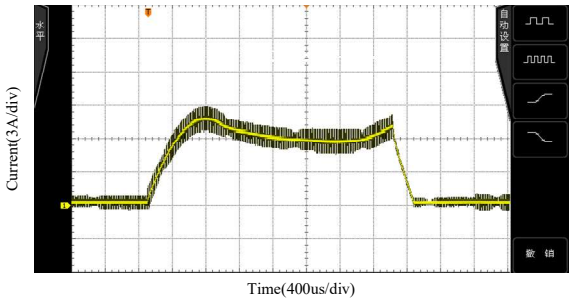

Fig. 20. The current waveform diagram of improved DITC method.

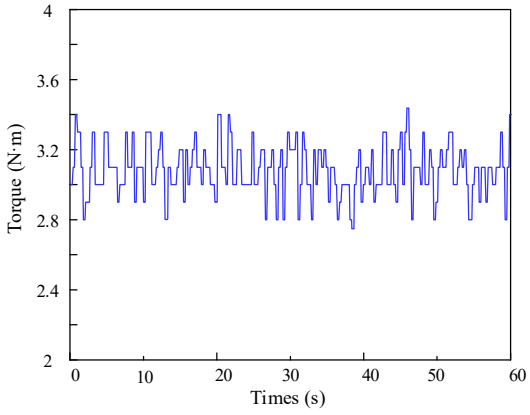

Fig. 21. The torque waveform diagram of improved DITC method.

the experimental results of the two control methods are shown in Fig. 22-25. As can be seen from Fig. 22-23, the peak current of conventional DITC is about 15 A, the torque is in the range of 6.46-4.55 N·m, and the torque ripple is 38.2%. It can be seen from Fig. 24~25 that the peak current of the improved DITC control method is about 10A, the torque is in the range of 5.45-4.7 N·m, and the torque ripple is 15%. Comparing the torque ripple under two control methods, it can be seen that the improved DITC control method can effectively reduce the torque ripple.

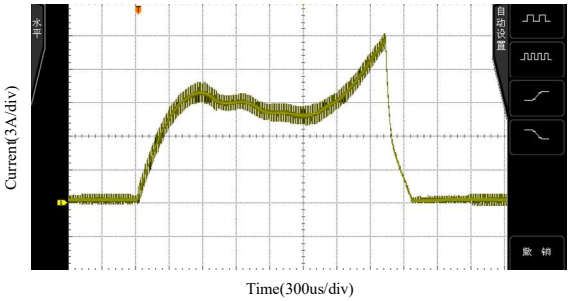

Fig. 22. The current waveform diagram of conventional DITC method.

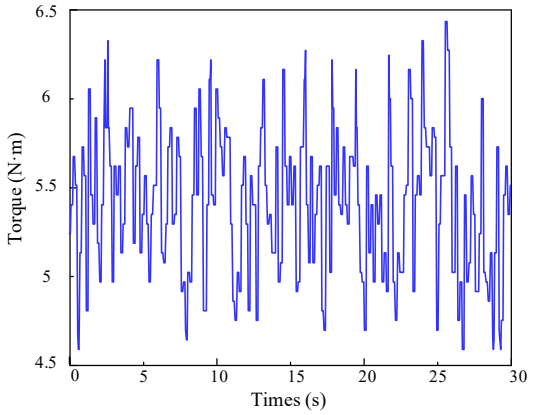

Fig. 23. The torque waveform diagram of conventional DITC method.

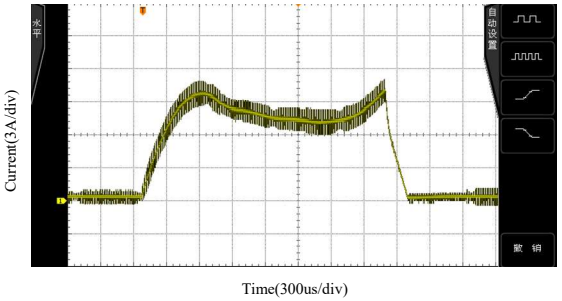

Fig. 24. The current waveform diagram of improved DITC method.

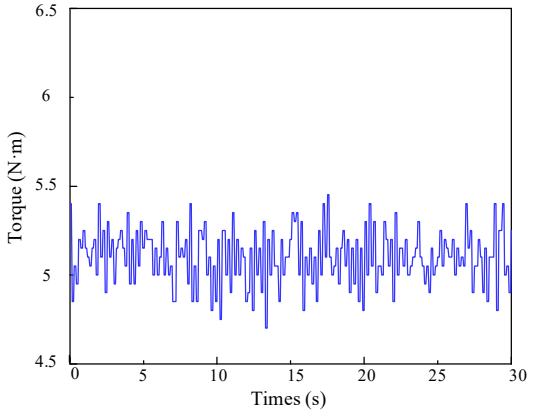

Fig. 25. The torque waveform diagram of improved DITC method.

VIII. CONCLUSION

In order to reduce the torque ripple of the DITC control

method during SRM operation. An improved DITC control method based on turn-on angle optimization is proposed. The improved GRNN neural network is used to design the algorithm of turn-on angle. At the same time, the two-phase exchange region is divided into two regions according to the inductance change rate, and different control schemes are designed in the regions. The following conclusions can be obtained through simulation analysis and experimental verification:

1) The GRNN neural network is improved by using K-fold cross verification algorithm, which improves the fitting accuracy of the neural network. The improved neural network can get the corresponding turn-on angle according to the speed and load torque.

2) According to the inductance change rate, the two-phase exchange area is divided into two regions. In each region, the one with larger inductance change rate and current is preferred to provide torque, which further reduces the torque ripple.

3) Compared with the conventional DITC control method, the torque ripple of the improved DITC control method is reduced by 15% and 23% respectively under different working conditions.

REFERENCES

[1] J. W. Ahn, and G. F. Lukman, "Switched Reluctance Motor: Research Trends and Overview," *CES Transactions on Electrical Machines and Systems*, vol. 2, no. 4, pp. 339-347, 2018.

[2] H. Cai, H. Wang, and M. Q. Li *et al* "Position Sensorless Control of Switched Reluctance Motors Considering the Magnetic Saturation," *Transactions of China Electrotechnical Society*, vol. 2, no. 12, pp. 2723-2734, 2018.

[3] X. Zhao, A. Xu, and W. Zhang, "Research on DTC System with Variable Flux for Switched Reluctance Motor," *CES Transactions on Electrical Machines and Systems*, vol. 1, no. 2, pp. 199-206, 2017.

[4] M. I. Mosaad, N. I. Elkalashy, and M. G. Ashmawy, "Integrating Adaptive Control of Renewable Distributed Switched Reluctance Generation and Feeder Protection Coordination," *Electric Power Systems Research*, vol. 154, pp. 452-462, 2018.

[5] G. Radhakrishnan, "Dual Mode Operation of 8/6 SRM with Optimum Angle Operation in Hybrid Electric Vehicles using FLC based Controller," *IOP Conference Series: Materials Science and Engineering*, vol. 623 pp. 012003, 2019.

[6] P. Constantin, C. Hao, and G.Yassen *et al*, "Artificial Neural Network Identification Model of SRM 12-8," *Procedia Earth and Planetary Science*, vol. 1, no. 1, pp. 1301-1311, 2009.

[7] R. B. Inderka, and R. W. A. A. De Doncker, "DITC-direct Instantaneous Torque Control of Switched Reluctance Drives," *IEEE Transactions on Industry Applications*, vol. 39, no. 4, pp. 1046-1051, 2003.

[8] K. F. Wong, K. W. E. Cheng, and S. L. Ho, "On-line Instantaneous Torque Control of a Switched Reluctance Motor Based pn Co-energy Control," *IET Electric Power Applications*, vol. 3, no. 4, pp. 257-264, 2009.

[9] N. H. Fuengwarodsakul, M. Menne, and R. B. Inderka *et al*, "High-dynamic Four-quadrant Switched Reluctance Drive Based on DITC," *IEEE Transactions on Industry Applications*, vol. 41, no. 5, pp. 1232-1242, 2005.

[10] J. Liang, D. H. Lee, and J. W. Ahn, "Direct Instantaneous Torque Control of Switched Reluctance Machines Using 4-level Converters," *IET Electric Power Applications*, vol. 3, no. 4, pp. 313-323, 2009.

[11] C. Gan, J. Wu, and Q. Sun *et al*, "Low-cost Direct Instantaneous Torque Control for Switched Reluctance Motors with Bus Current Detection under Soft-chopping Mode," *IET Power Electronics*, vol. 9, no. 3, pp. 482-490, 2016.

[12] R. Mikail, I. Husain, and Y. Sozer *et al*, "Torque-ripple Minimization of Switched Reluctance Machines Through Current Profiling," *IEEE Transactions on Industry Applications*, vol. 49, no. 3, pp. 1258-1267, 2013.

[13] V. P. Vujičić, "Minimization of Torque Ripple and Copper Losses in Switched Reluctance Drive," *IEEE Transactions on Power Electronics*, vol. 27, no. 1, pp. 388-399, 2012.

[14] J. Ye, B. Bilgin, and A. Emadi, "An Offline Torque Sharing Function for Torque Ripple Reduction in Switched Reluctance Motor Drives," *IEEE Transactions on Energy Conversion*, vol. 30, no. 2, pp. 726-735, 2015.

[15] Q. Sun, J. Wu, and C. Gan *et al*, "OCTSF for Torque Ripple Minimisation in SRMs," *IET Power Electronics*, vol. 9, no. 14, pp. 2741-2750, 2016.

[16] M. Ma, K. Yuan, and Q. Yang *et al*, "Open-circuit Fault-tolerant Control Strategy Based on Five-level Power Converter for SRM System," *CES Transactions on Electrical Machines and Systems*, vol. 3, no. 2, pp. 178-186, 2019.

[17] J. Deskur, T. Paichrowski, and K. Zawirski, "Optimal Control of Current Switching Angles for High-speed SRM Drive," *Compel-the International Journal for Computation and Mathematics in Electrical and Electronic Engineering*, vol. 29, no. 1, pp. 156-172, 2010.

[18] M. Hamouda, A. A. Menaem, and H. Rezk *et al*, "Comparative Evaluation for an Improved Direct Instantaneous Torque Control Strategy of Switched Reluctance Motor Drives for Electric Vehicles," *Mathematics*, vol. 9, pp. 4, 2021.

[19] T. Chen, and G. Cheng, "Comparative Investigation of Torque-ripple Suppression Control Strategies Based on Torque-sharing Function for Switched Reluctance Motor," *CES Transactions on Electrical Machines and Systems*, vol. 6, no. 2, pp. 170-178, 2022.

[20] Z. Zhang, S. Rao, and X. Zhang, "Performance Prediction of Switched Reluctance Motor Using Improved Generalized Regression Neural Networks for Design Optimization," *CES Transactions on Electrical Machines and Systems*, vol. 2, no. 4, pp. 371-376, 2018.

[21] C. L. Xia, Z. R. Chen, and B. Li, "Instantaneous Torque Control of Switched Reluctance Motors Based on RBF Neural Network," *Proceedings of the Chinese Society of Electrical Engineering*, vol. 4, no.19, pp. 127-132, 2006.

[22] B. N. Qu, S. C. Song, and J. C. Song *et al*, "Switch Angle Optimization Method for Switched Reluctance Motor Considering the Inductance Variation in Small Inductance Period," *Electric Machines and Control*, vol. 3, no.2, pp. 87-93, 2019.

Chaozhi Huang was born in 1978 and received the B.S. degree in 2001. He received the M.S. degrees in detection technology and automation from Jiangxi University of Science and Technology, Ganzhou, China, in 2004. Later, he received the Ph. D degrees in Power System and Automation from Hohai University.

Since 1998, he has been with Jiangxi University of Science and Technology, where he is currently a professor in the School of Electrical Engineering and Automation. His research interests include motor structure design and drive control, robot control technology.

Wensheng Cao was born in Shanxi, China, in 1997. He received the B.S. degree in automation department from Taiyuan Industry College in 2020. He is currently working toward the M.S. degree in the electronic information from Jiangxi University of Science and Technology since 2020.

His research interests include the drive and control of switched reluctance motor.

Zhou Chen was born in Jiangxi, China, in 1998. He received the B.S. degree in electrical engineering from Jiangxi University of Science and Technology in 2021. He is currently working toward the M.S. degree in the electrical engineering from Jiangxi University of Science and Technology.

His current research interests include the drive and control of switched reluctance motor.

Yuliang Wu was born in Sichuan, China, in 1996. He received the B.S. degree in electrical engineering from Shanxi Agricultural University in 2019. He is currently working toward the M.S. degree in the electronic information from Jiangxi University of Science and Technology.

His current research interests include motor drive and control.

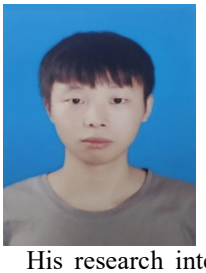

Yongmin Geng was born in Henan, China, in 1997. He received the B.S. degree in electrical engineering from Henan Institute of Science and Technology in 2019. He is currently working toward the M.S. degree in electrical engineering from Jiangxi University of Science and Technology since 2020.

His research interests include optimal design of electrical machine structures.